# EFFECT OF THE BUILD DIRECTION ON DEFECT DISTRIBUTION AND CRACK INITIATION OF LPBF TI6AL4V

Wenbo Sun[1], Yu'e Ma[2] and Weihong Zhang[1]

[1] School of Mechanical Engineering, Northwestern Polytechnical University, 710072, Xi'an, P.R.China and wenbo-sun@nwpu.edu.cn
[2] School of Aeronautics, Northwestern Polytechnical University, 710072, Xi'an, P.R.China

**Abstract:** Additive manufactured (AM) Ti6Al4V titanium alloy has a great prospect to manufacture complex aircraft structures. A relatively better static mechanical performance of AM metal materials has been achieved by the optimized processing parameters. The defects are inevitable characteristics in AM alloys, and it can be affected by the processing parameters and post-treatment. A comprehensive study on the defect characterization and its effect on crack initiation behaviour were performed in this paper. Laser powder bed fused (LPBF) Ti6Al4V titanium alloy in 0°, 45°, and 90° build directions were designed and manufactured. The defects were measured based on X-ray computed tomography and reconstructed using the Dragonfly software. The defect distributions along the radial direction were compared. Defect size and defect orientation were characterized. Finally, the real defects were extracted and imported into a finite element model, effects of the defect orientation and the porosity on crack path were analysed. It was shown that the porosity of the stress relieved samples decreased firstly and then increased with the enlargement of the build direction. The lack of fusion defects is prone to growing along the build direction. The crack initiation site was controlled by the defect orientation and the effective bearing aera.

**Keywords:** Laser powder bed fused; Additive manufacturing; Build direction; Defect distribution; Crack initiation

## INTRODUCTION

Additive manufactured (AM) Ti6Al4V titanium alloy has has drawn much attention in aerospace industries due to its excellent properties, such as higher specific strength and corrosion resistance. Compared with the conventionally manufactured parts, a finer microstructure of AM metal materials can be produced by using these optimized processing parameters. And this can result in a relatively better static mechanical performance. However, the defects in AM metal alloy cannot be eliminated thoroughly, and defects can lead to the degradation of fatigue properties and the anisotropic mechanical response [1-4].

During manufacturing, the powders were deposited on the top of the substrate materials, and then melted by the laser beam. For additive manufacturing, lack of fusion (LoF) and porosity defects are inevitable due to different input energy densities and the complexity of the coupling of the multi-physics

fields [5]. Incomplete melting will cause LoF defects with large, irregular, and sharp shape, while over melting will cause trapped gas porosity and keyholing with a near-spherical morphology [6]. LoF defects are prone to appearing at the remaining laser track between the adjacent laser paths and the consecutive depositions because the liquid metal shrinks during colling[1, 7]. The coalescence and agglomeration of the defects can be observed in the subsurface region and the support connected areas, where the unstable energy inputting can increase porosity [2, 8].

The maneuverability of additive manufacturing makes it possible to reduce the porosity by changing the processing parameters [9] and the contouring passes [10]. Several researchers have studied the effect of processing parameters on porosity [2, 5-7, 9], and the energy density $E_v$ can be used to optimize the total porosity of AM alloy as a ratio between the laser power $P$, the scanning speed $v$, the hatch distance $h$, and the layer thickness $t$:

$$E_v = \frac{P}{v \cdot h \cdot t} \tag{1}$$

The defect size decreases with a steep slope as the energy density increases to a certain value, and then starts to increase with a lower slope with a further increase in the energy density [5, 6]. The porosity of AM alloy can be effectively eliminated by optimized processing parameters, the new subsequent layer and thermal cycle [11, 12], and the laser power and velocity are two dominant factors [8, 13]. Du [9] found that laser power has the biggest effect on the porosity, while Kasperovich [5] found that the velocity exerts the most dominant influence on the porosity fraction. In addition, the melt pool characterization, such as the melt pool area [14] and the solidification [15] also has a profound effect on the defect.

X-ray computed tomography technique is an efficient method to get the 3-D reconstruction of the defect information in AM metal alloy. The population of defects was dominated by the trapped gas pores, but the crack and damage initiation of AM alloy resulted from the LoF defects which are distributed in the indications of insufficient melting in track-track or layer-layer overlapping [9] and formed perpendicular to the build direction [16]. Seifi [17] used the boxplots to correlate defect size to the build height and found that the largest defect size was almost in the middle section of the sample, which can be caused by the transient thermal evolution [18]. According to the difference in sample size and the accuracy of the measuring equipment, the statistical distribution of pores can be fitted by the normal distribution [19], the exponential distribution [20], and the logarithmic normal distribution [21-23]. Small defects will be neglected when analyzing the effect of the defect on the mechanical performance of AM alloy, and the logarithmic normal distribution is more suitable. In addition, Xu [24] characterized the defect $\sqrt{aera}$ by the Weibull distribution function and found the 45° sample has a higher defect size than the 0° sample and the 90° sample. Both sphericity and aspect ratio of the AM metal defects typically decreased with increase of the defect size [11].

Due to the inability to fully eliminate defects in AM metal materials, the characteristics of defects, such as size, location, and distribution, should be studied carefully and thoroughly. In addition, the effect of the build direction on defect distribution also needs to be considered. In this paper, laser powder bed fused (LPBF) Ti6Al4V titanium alloy in 0°, 45°, and 90° build direction were designed and manufactured, stress relieving process was conducted. The defects were measured based on the X-ray computed tomography and reconstructed using the Dragonfly software. The defect distributions of the stress relieved sample along the radial direction were compared. Defect size and defect orientation were characterized. Finally, a finite element model with the real defects were established, and the crack initiation site and the crack path of the three build direction samples were simulated.

## MATERIALS AND METHODS

### Sample design

The LPBF Ti6Al4V cylindrical specimens in 0°, 45°, and 90° build directions were designed and

fabricated. The diameter of all samples is around 3 cm. The BLT-TC4 powder were used, and the chemical compositions of the Ti6Al4V powder are listed in Table 1. All samples were manufactured by a BLT-S310 machine with a 350 W laser. The laser beam diameter was 0.08 mm, and the scanning speed was 1000 mm/s. A cross-hatch pattern scanning strategy was used with a 60 μm of layer thickness and 200 μm of hatch spacing. To ensure that build direction was the only factor, all specimens were printed independently and post-processed in the same condition. A stress relief heat treatment process was performed once the specimens were manufactured. All specimens were annealed for 4 hours at 800±5 ℃, and then cooled in Argon gas to room temperature.

Table 1 Chemical compositions of Ti6Al4V powders (wt %)

| (%) | | | | | | | |
|---|---|---|---|---|---|---|---|
| Ti | Al | V | Fe | C | H | O | N |
| balance | 5.5-6.75 | 3.5-4.5 | ≤0.30 | ≤0.08 | ≤0.015 | ≤0.20 | ≤0.05 |

Defect analysis

X-ray computed tomography (CT) is a non-destructive industrial inspection method that can determine the inner, small, and irregular defects of AM part. The porosity and defects of LPBF Ti6Al4V titanium alloy in three build directions were detected using an X-ray CT modeled as ZEISS Xradia 520 Versa. The CT characterization has a resolution of 5.89 μm per voxel to capture small-scale defects with a diameter of 10 μm or larger.

Dragonfly software was used to reconstruct the spatial distribution of AM defects obtained by X-ray. Quantitative information, such as the defect volume and the defect coordinate both can be imported and analyzed. The Feret diameter was measured to character the defect size, and this diameter is not in its actual sense but the common basis of a group of diameters derived from the distance of two tangents to the contour of the defect in a well-defined orientation. √area, a representative parameter for defect in fatigue analysis of metal alloy, is defined as the square root of defect projected aera on the deposition plane (along the build direction), and the irregularly projected shaped of single defect was regarded as an ellipse.

## RESULTS AND DISCUSSION

Spatial distribution and porosity

The spatial distributions with respect to the $\sqrt{area}$ of all samples are shown in Figure 1, and its geometrical dimensions and defect statistics are listed in Table 2. The proportion of larger size defects in all samples is small. It is shown that both the counts and total volume of the defect in the 45° sample are the lowest, as shown in Figure 1(b). The defect distribution of the 90° sample is relatively uniform compared with the other two build direction samples, shown in Figure 1(c). The maximum$\sqrt{area}$ value of the 0° sample and the 90° sample is about 330 μm, while that value of the 45° sample (280 μm) is the smallest. Corresponding, the 45° sample has the lowest porosity of 1.55%, while the 90° sample is more than 2 times higher than that. The relationship between the porosity and the build direction are shown in Figure 1(d). The build direction can change the defect size and distribution of LPBF Ti6Al4V titanium alloy.

When a new layer was built, the repeated thermal history in the substrate deposited layers can make the defects remelt and heal, and then the defect with an inverted cone shape will present, especially these long and large defects. In addition, different temperature gradient in three build direction samples also has a significant effect on the defect distribution and the porosity. When stress relieving was performed, high temperature condition can cause the coalescence of initial cracks into a bigger one. This phenomenon more easily appeared in the 90° sample because of the higher number of defects. Consequently, a noticeable improvement of the porosity in the 90° stress relieved sample can be obtained.

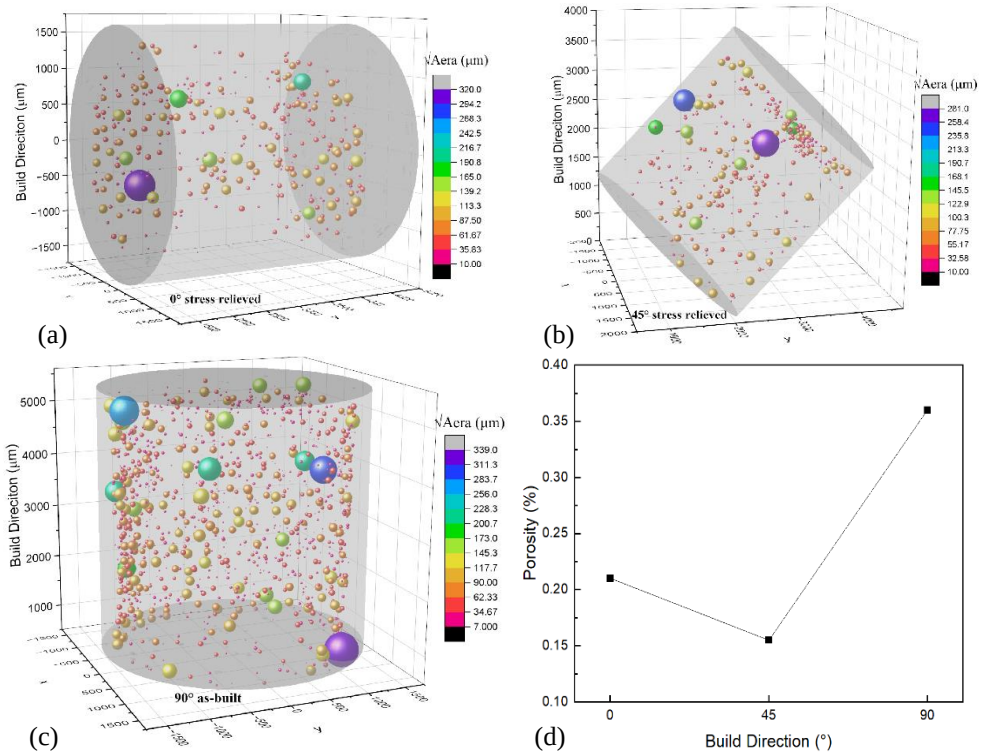


Figure 1 Defect distribution and porosity: (a) the 0° sample, (b) the 45° sample, (c) the 90° sample, (d) the porosity

Table 2 Geometry and defect data of the stress relieved samples

| Build Direction | Max Feret Diameter (μm) | Total Volume (μm³) | Counts | Porosity (%) |
|---|---|---|---|---|
| 0° | 506 | 3.75 E7 | 362 | 0.210 |
| 45° | 495 | 2.85 E7 | 335 | 0.155 |
| 90° | 730 | 1.14 E8 | 1160 | 0.360 |

Defect distribution along the radial direction

The porosity distribution along the radial direction is essential to the mechanical property of AM metal, especially the fatigue behavior. It is obvious that porosity near the subsurface region is much higher than that of the other regions, and the defect orthogonal projection distribution of three build direction samples along the axial direction are compared, shown in Figure 2. An apparent agglomeration of defects near the cylindrical surfaces were observed in the 90° sample, shown in Figure 2(c), while large defects also can be observed at the center of the radial orthographic projection of the 0° sample in Figure 2 (a) and the 45° sample in Figure 2(b), and these defects are located on the end face of the samples, shown in Figure 1.

Statistical analysis was performed on defects with √area value larger than 80 μm, and the relative frequency versus distance form the surface were plotted in Figure 2(d). All samples had a higher porosity in the subsurface region, which is about 5 times as high as that of the other regions, and even more than 10 times for the 90° stress relieved sample, shown in Figure 2(d). It can be concluded that the defect coalescence phenomenon caused by the stress relieving process is mainly concentrated in the subsurface region.

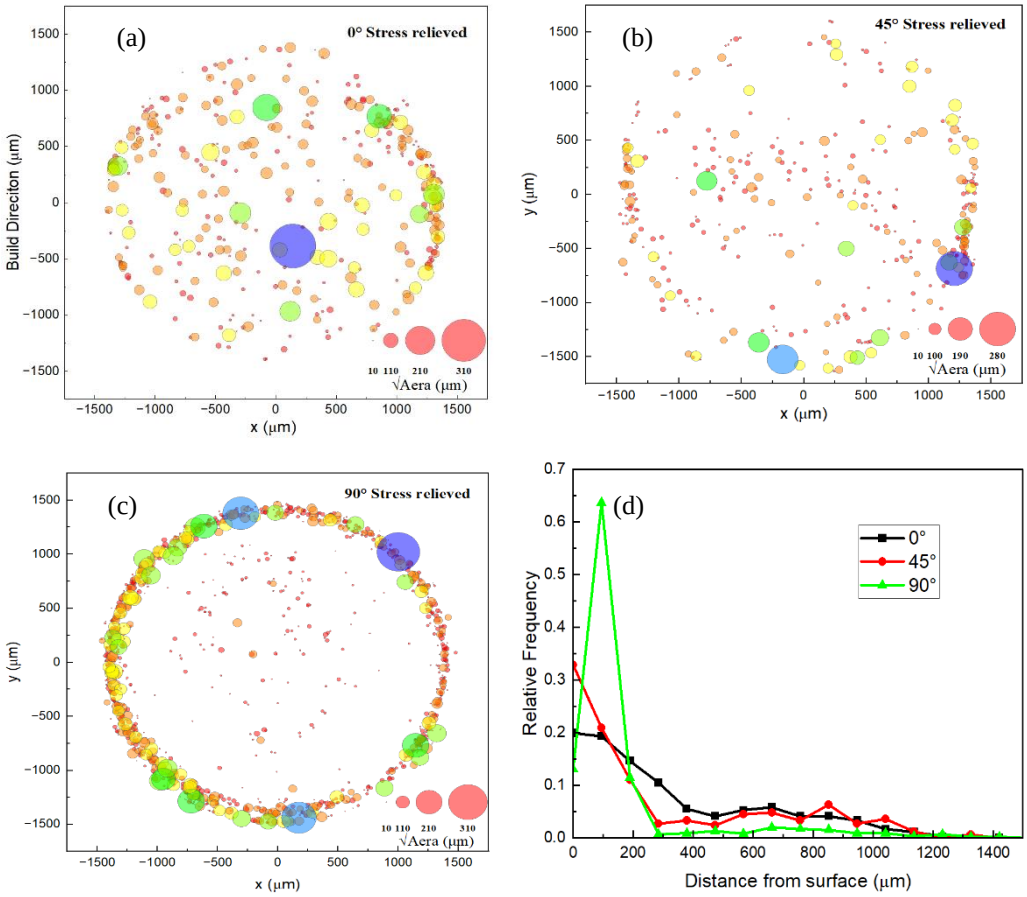


Figure 2 Defect distribution along the radial direction: (a) the 0° sample, (b) the 45° sample, (c) the 90° sample, (d) relative frequency

Defect orientation

The difference of defect orientation is of great significance to the crack initiation and propagation. Therefore, the direction of defect is analyzed statistically. In Dragonfly, the defect orientation is determined by an eigenvector associated with the smallest eigenvalue of the inertia tensor, which represents the axis of easiest rotation, and the long axis of the defect. The defect orientation in this section is defined as the angle between the major axis of the defect and the build direction. It means that the smaller the angle is, the more the defects are distributed along the build direction, while the defect with a large angle distributed along the scanning direction.

The percentage of defect orientation distribution and the illustration of defect orientation are shown in Figure 3. For the 0° sample in Figure 3(a), the defect orientations are mostly distributed in the range of 0-20 degree, while that of the 45° sample are in the range of 70-90 degree, shown in Figure 3(b). The defect orientation of the 90° sample is relatively uniform in each interval, shown in Figure 3(c). Larger defects presented both in these three build direction samples with an irregular shape, but are prone to growing along the axial direction of the cylindrical sample. The effect of the build direction on the defect orientation distribution can be attributed to the change of cross-sectional gradient during the printing process. When stress relieving was performed, the adjacent small defects will coalesce and change the defect orientation under high temperature.

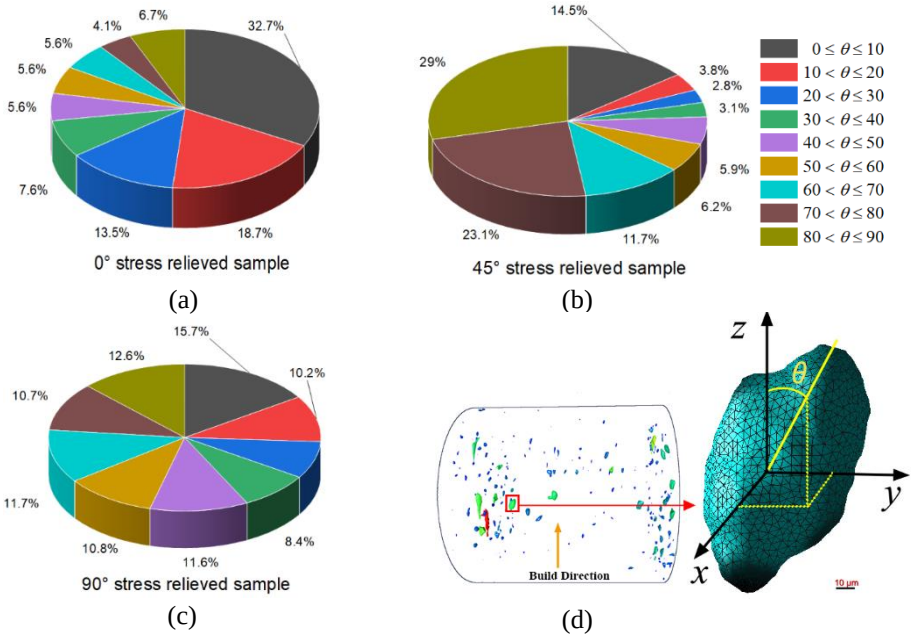


Figure 3 Defect orientation

Simulation

A finite element model was established to study the effect of the defect on crack initiation and crack path. Axial sections with the real defects of the three build direction samples were extracted and meshed, and a uniaxial tensile load was applied. The mechanical and damage parameters of these three samples are derived from our previous experimental data[25, 26].

The simulated results are shown in Figure 4, and the effective bearing aera distribution along the loading direction are also given. For the 0° sample, the crack initiated from a subsurface defect, rather than the defect located in the section with a minimum effective bearing area. For the 45° sample, the material began to crack due to defect orientation and small effective bearing area, and these two coupling effects make it not crack from the surface defect. There are two sites with close effective bearing area in the 90° sample, and the defect size and the distance from the surface are also similar. In this situation, the crack orientation plays an important role.

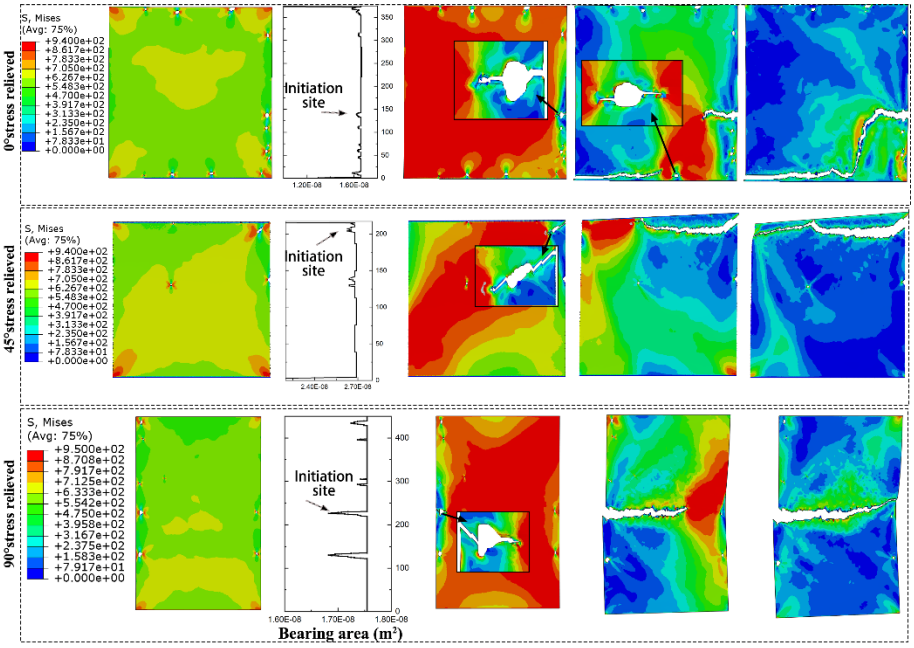


Figure 4 Crack initiation and crack path

## CONCLUSION

In this paper, the spatial distribution of defects in LPBF Ti6Al4V titanium alloy was characterized. Effects of the build direction were analyzed, and the main conclusions are drawn as follows:

(1) The defect distribution can be reconstructed with a diameter of 10 μm based on X-ray computed tomography. The porosity of the stress relieved samples decreased firstly and then increased with the enlargement of the build direction. The 90° sample has the highest porosity with a value of 0.36%.

(2) Larger defects are prone to agglomerating in the subsurface region. The effects of the build direction on the defect distribution and the orientation are mainly due to the different temperature gradient caused by the cross-section change during printing. And the stress relieving also can lead to the small defect coalescence and change the defect orientation.

(3) Defect orientation and the effective bearing area are two importance factors that can affect the crack initiation site and crack path.

## REFERENCES

[1] D. Svetlizky, M. Das, B. Zheng, A. L. Vyatskikh, S. Bose, A. Bandyopadhyay, J. M. Schoenung, E. J. Lavernia, N. Eliaz. (2021), *Mater. Today*, 49:271-295.
[2] A. du Plessis, I. Yadroitsava, I. Yadroitsev. (2020), *Mater. Des.*, 187:108385.
[3] H. Li, Z. Tian, J. Zheng, K. Huang, B. Nie, W. Xu, Z. Zhao. (2023), *Int. J. Fatigue*, 167:107375.
[4] D. Hu, J. Pan, D. Mi, J. Mao, W. Li, Y. Fu, R. Wang. (2022), *Int. J. Fatigue*, 158:106734.
[5] G. Kasperovich, J. Haubrich, J. Gussone, G. Requena. (2016), *Mater. Des.*, 105:160-170.
[6] N. Sanaei, A. Fatemi. (2020), Materials Science and Engineering: A, 785:139385.
[7] C. Xie, S. Wu, Y. Yu, H. Zhang, Y. Hu, M. Zhang, G. Wang. (2021), *J. Mater. Process. Technol.*, 291:117039.
[8] W. Liu, C. Chen, S. Shuai, R. Zhao, L. Liu, X. Wang, T. Hu, W. Xuan, C. Li, J. Yu, J. Wang, Z. Ren. (2020), Materials Science and Engineering: A, 797:139981.
[9] L. Du, G. Qian, L. Zheng, Y. Hong. (2021), *Fatigue Fract. Eng. Mater. Struct.*, 44(1):240-256.
[10] T. Childerhouse, E. Hernández-Nava, N. Tapoglou, R. M Saoubi, L. Franca, W. Leahy, M. Jackson. (2021), *Int. J. Fatigue*, 147:106169.
[11] N. Sanaei, A. Fatemi. (2021), Prog. Mater. Sci., 117.
[12] C. H. Ng, M. J. Bermingham, M. S. Dargusch. (2021), *Addit. Manuf.*, 39:101855.
[13] T. P. Moran, D. H. Warner, N. Phan. (2021), *Addit. Manuf.*, 37:101667.
[14] R. Cunningham, S. P. Narra, T. Ozturk, J. Beuth, A. D. Rollett. (2016), *Jom*, 68(3):765-771.
[15] T. Hauser, R. T. Reisch, P. P. Breese, B. S. Lutz, M. Pantano, Y. Nalam, K. Bela, T. Kamps, J. Volpp, A. F. H. Kaplan. (2021), *Addit. Manuf.*, 41:101993.
[16] M. J. Mian, J. Razmi, L. Ladani. (2021), *Materialia*, 16:101041.
[17] M. Seifi, A. Salem, D. Satko, J. Shaffer, J. J. Lewandowski. (2017), Int. J. Fatigue, 94:263-287.
[18] J. Ge, T. Ma, W. Han, T. Yuan, T. Jin, H. Fu, R. Xiao, Y. Lei, J. Lin. (2019), *Appl. Therm. Eng.*, 163:114335.
[19] R. S. Haridas, S. Thapliyal, P. Agrawal, R. S. Mishra. (2020), Materials Science and Engineering: A, 798:140082.
[20] S. Romano, A. Abel, J. Gumpinger, A. D. Brandão, S. Beretta. (2019), *Addit. Manuf.*, 28:394-405.
[21] D. Hu, J. Pan, J. Mao, S. Hu, X. Liu, Y. Fu, R. Wang. (2021), *Mater. Des.*, 198:109353.
[22] Y. N. Hu, S. C. Wu, Z. K. Wu, X. L. Zhong, S. Ahmed, S. Karabal, X. H. Xiao, H. O. Zhang, P. J. Withers. (2020), *Int. J. Fatigue*, 136:105584.
[23] Y. N. Hu, S. C. Wu, P. J. Withers, J. Zhang, H. Y. X. Bao, Y. N. Fu, G. Z. Kang. (2020), *Mater. Des.*, 192:108708.
[24] Z. Xu, A. Liu, X. Wang, B. Liu, M. Guo. (2021), *Int. J. Fatigue*, 143:106008.

[25] W. Sun, Y. Ma, W. Huang, W. Zhang, X. Qian. (2020), *Int. J. Fatigue*, 130:105260.
[26] W. Sun, Y. E. Ma, W. Zhang, X. Qian, W. Huang, Z. Wang. (2021), *Adv. Eng. Mater.*, 23(12):2100611.